ARTICLES

Multiconfiguration resonating-group theory of ^{8}Li

Y. Fujiwara*
Theoretical Physics Institute, School of Physics, University of Minnesota, Minneapolis, Minnesota 55455 and Department of Physics, Kyoto University, Kyoto 606, Japan

Y. C. Tang
School of Physics, University of Minnesota, Minneapolis, Minnesota 55455
(Received 28 August 1989)

The nucleus ^{8}Li is studied with a multiconfiguration resonating-group calculation which consists of $n+^7$Li, $t+^5$He, $n+^7$Li*, and ^{4}H$+\alpha$ cluster configurations. With no adjustable parameters, the results show that the calculated level spectrum agrees well with experiment and with the empirical level spectrum obtained by Knox, Resler, and Lane using an extensive R-matrix analysis. A calculation employing only the $n+^7$Li configuration is found to be generally inadequate. Among the configurations $t+^5$He, $n+^7$Li*, and ^{4}H$+\alpha$ which are employed to enlarge the model space, the $n+^7$Li* configuration is shown to be the most important from an overall viewpoint. Comparisons between calculated and experimental scattering and reaction cross sections have also been made. Here one finds that the calculation explains all the main features of measured results. In particular, the triton production cross section of the ^{7}Li$(n,n't)\alpha$ reaction is well reproduced. The calculated $n+^7$Li total reaction cross section turns out to be somewhat too small, being equal to around 75% of the experimental value.

I. INTRODUCTION

Recently, we have made a detailed investigation[1] of the essential properties of the seven-nucleon system using a three-cluster resonating-group formulation. In that investigation, the two-cluster configurations included in the calculation are $t+\alpha$, $n+^6$Li, and $n+^6$Li* configurations, with ^{6}Li* being the $T=0$ excited state of ^{6}Li having a $d+\alpha$ cluster structure with relative orbital angular momentum equal to 2 (the $d+^5$He cluster configuration is also considered in some parts of the calculation[1,2]). To insure the reliability of the results, we have carefully chosen the cluster internal functions not only to take proper consideration of the nucleon correlation structure and the form-factor behavior of the clusters, but also to satisfy rather well the variational stability condition. With these precautions and the use of a rather large model space, the results did turn out to be quite satisfactory. It was found that the calculated level spectrum agrees well with the spectrum determined empirically by Knox and Lane[3] with a careful R-matrix analysis of experimental data, and that the essential characteristics of the oscillatory patterns exhibited in cross-section angular distributions can be reasonably explained.[4] More interestingly, we have also learned from this calculation the cluster structures of the bound and resonance levels, and the basic behavior of the intricate interplay among various cluster configurations.

The success in the seven-nucleon calculation encourages us to proceed and investigate the neighboring system ^{8}Li. For this investigation, we shall adopt an $n+t+\alpha$ three-cluster formulation[5] and derive from it coupled-channel equations involving two-cluster $n+^7$Li, $n+^7$Li*, $t+^5$He, and ^{4}H$+\alpha$ configurations, where ^{7}Li* denotes the excited state of ^{7}Li having a $t+\alpha$ cluster structure and is the rotational partner of ^{7}Li in its ground state. Here again, the main purpose is to see how well a large-model-space calculation can explain the essential properties of this nuclear system, regarding the cluster structures of the levels, reaction mechanisms, and so on. In addition, there are also some practical aspects associated with this investigation; for example, the reaction ^{7}Li$(n,n't)\alpha$ is important for tritium breeding in the design of fusion reactors.[6]

Comparison with experiment is facilitated by the existence of a multilevel, multichannel R-matrix analysis[7] of measured cross sections for reactions leading to the compound system ^{8}Li. This particular analysis has a semimicroscopic nature, in the sense that information obtained from shell-model calculations is also utilized. In addition to the usual application of providing reliable values for level parameters, it has also the important feature of predicting cross-section results for reactions, such as the ^{7}Li$(n,t)^5$He reaction, where no experimental data are yet available.

The ^{8}Li system has also been previously investigated. Using the resonating-group-equivalent generator-coordinate method, Descouvemont and Baye[8] have studied this system with a single $n+^7$Li cluster configuration. The results that they obtained did yield qualitatively use-

ful information; but their chosen model space is clearly too small, as is evidenced by the fact that the experimentally well-established $J^\pi=4^+$ level at 6.53-MeV excitation[9,10] cannot be found in this investigation. In the resonating-group study of Stöwe and Zahn,[11] the model space is larger, being spanned by both $n+^7$Li and $t+^5$He cluster configurations. However, even with such a model space, our calculation shows that their omission of, in particular, the $n+^7$Li* cluster configuration is a significant defect that resulted in some rather undesirable consequences.

The outline of this paper is as follows. In Sec. II, we briefly describe the formulation, the nucleon-nucleon potential used, and the choice of cluster internal functions. Results for phase shifts and transmission coefficients are discussed in Sec. III, while those for cross sections are discussed in Sec. IV. Finally, in Sec. V, we summarize the findings of this study and make some concluding remarks.

II. FORMULATION OF THE ^{8}Li PROBLEM

A. Brief discussion of the formulation

Similar to the ^{7}Li case discussed previously,[1] the ^{8}Li system will first be formulated as an $A+B+C$ three-cluster system, with A, B, and C representing α, t, and n clusters, respectively. From the three-cluster kernel derived,[12] coupled-channel equations, involving two-cluster $(A+B)+C$, $(A+C)+B$, and $A+(B+C)$ configurations, are then obtained by choosing appropriate relative-motion functions for the $(A+B)$, $(A+C)$, and $(B+C)$ subsystems. These coupled equations are eventually solved by using a variational technique employing Gaussian-type trial functions.[13] For all these steps, thorough discussions have already been given in a previous report;[5] hence, they will not be further described here.

In this case, the two-cluster configurations included in the calculation are $n+^7$Li, $t+^5$He, $n+^7$Li*, and ^{4}H$+\alpha$ configurations, with ^{7}Li* being the excited state of ^{7}Li that has predominantly a $t+\alpha$ cluster structure and is the rotational partner of ^{7}Li in its ground state. These will be referred to as cluster configurations a, b, c, and d, respectively. Cluster configurations, such as ^{6}Li$+2n$ and ^{6}He$+d$, are not included in this investigation. The inclusion of these configurations will require the further addition of an $\alpha+d+2n$ three-cluster term in the formulation and, thereby, vastly increase the computational complexity. In any case, it is our belief that the Pauli principle has the important effect of greatly reducing the differences between seemingly different cluster structures when the nucleons are in close proximity; hence, the omission of these particular cluster configurations is not expected to result in drastic consequences.

In our three-cluster formulation,[5] there exists the restriction that all constituent clusters have to be described by translationally invariant shell-model functions of the lowest configuration in harmonic-oscillator wells of the same width parameter. For our case, this common width parameter is most appropriately chosen to be equal to 0.514 fm^{-2}, in order to yield correctly the empirically determined root-mean-square (rms) matter radius of 1.48 fm for the α particle.

The nucleon-nucleon potential employed in this investigation is the Minnesota or MN potential[14] with the exchange-mixture parameter u set to be equal to one. This potential is given by Eqs. (9)–(11) in Ref. 14, and has been used[1,2,15] to obtain successful results in the neighboring nucleus ^{7}Li. To reduce computational effort, we have, as in Ref. 1, not considered the Coulomb interaction and effects arising from noncentral forces. The omission of an explicit consideration of the Coulomb force is a reasonable simplification, since the main concern in our present study is on the bound-state and phase-shift properties of the $n+^7$Li system and, being a long-range force, its effects can be easily estimated. As for noncentral spin-orbit and tensor forces, they are necessary for discussing detailed features of experimental data, but are not essential for studying the cluster structures of bound and resonance levels and for attempting to learn the basic behavior of the intricate interplay among various cluster configurations.

The adoption of a purely central nucleon-nucleon potential indicates that both the total orbital angular momentum L and the total spin angular momentum S ($S=0$ or 1) are good quantum numbers. Therefore, the values of these angular momenta can be used to characterize a particular channel wave function. In addition, for a complete characterization, it is of course also necessary to specify the cluster configuration (a, b, c, or d) and the relative orbital angular momentum l between the constituent clusters which couples with the cluster internal orbit angular momentum I ($I=1$, 1, 3, and 1 for clusters ^{7}Li, ^{5}He, ^{7}Li*, and ^{4}H, respectively) to yield the desired value of L.

The trial wave function in a particular (L,S) state is written as the linear superposition of a number of channel wave functions ψ_{lj}^{LS}, with the index j specifying the cluster configuration. These channel wave functions are

$$\psi_{la}^{LS}=\mathcal{A}\left\{\left[\left[\phi_7(I=1)\frac{1}{R_a}f_{la}^{LS}(R_a)Y_l(\hat{\mathbf{R}}_a)\right]_L \times\xi_{aS}Z(\mathbf{R}_{\text{c.m.}})\right\}, \tag{1}$$

$$\psi_{lb}^{LS}=\mathcal{A}\left\{\left[\left[\phi_t\phi_5(I=1)\frac{1}{R_b}f_{lb}^{LS}(R_b)Y_l(\hat{\mathbf{R}}_b)\right]_L \times\xi_{bS}Z(\mathbf{R}_{\text{c.m.}})\right\}, \tag{2}$$

$$\psi_{lc}^{LS}=\mathcal{A}\left\{\left[\left[\phi_7^*(I=3)\frac{1}{R_c}f_{lc}^{LS}(R_c)Y_l(\hat{\mathbf{R}}_c)\right]_L \times\xi_{cS}Z(\mathbf{R}_{\text{c.m.}})\right\}, \tag{3}$$

$$\psi_{ld}^{LS}=\mathcal{A}\left\{\left[\left[\phi_\alpha\phi_4(I=1)\frac{1}{R_d}f_{ld}^{LS}(R_d)Y_l(\hat{\mathbf{R}}_d)\right]_L \times\xi_{dS}Z(\mathbf{R}_{\text{c.m.}})\right\}, \tag{4}$$

with $\mathcal{A}$ being an antisymmetrization operator, ξ_{jS} being appropriate spin-isospin functions, $Z(\mathbf{R}_{\text{c.m.}})$ being any normalizable function describing the motion of the total center of mass, and $\mathbf{R}_j$ representing the intercluster separation distances. The normalized functions ϕ_n ($n=4$, 5, and 7) and ϕ_7^* describe the internal spatial structures of the various constituent clusters, with the subscript n denoting the number of nucleons within the cluster.

For a certain choice of L and parity, the orbital angular momentum l can take on one or more values. That is, there are, in general, more channels than cluster configurations. For example, consider $L=4$ and positive parity. Here the allowed values of l for cluster configurations a, b, and d are 3 and 5, and for cluster configuration c are 1, 3, 5, and 7. Thus, in this particular L^π state with S equal to either 0 or 1, the total number of channels is 10, if all four cluster configurations are included in the calculation.

To investigate the effects of enlarging the model space and to gain information about the cluster structures of bound and resonance levels, we perform the calculations in a number of model spaces, defined according to the cluster configurations included. In Table I, we list the various model spaces considered, with SC, DC, TC, and QC denoting single-configuration, double-configuration, triple-configuration, and quadruple-configuration calculations. Using this terminology, we note that the calculations reported in Refs. 8 and 11 were performed in the SC and DC1 spaces, respectively.

The linear variational amplitudes or relative-motion functions f_{lj}^{LS} are obtained by solving a set of coupled integro-differential equations.[16] From the results, we deduce the S-matrix elements S_{fi}^L in $S=0$ and 1 states, and, subsequently, calculate various scattering and reaction cross sections.

The initial channel i and the final channel f will be labeled by the value of the orbital angular momentum l and the type of cluster configuration j ($j=a$, b, c, or d). That is, they will be specified by a pair of indices (lj). For example, in the $L=3$ state, $S_{1c,3a}^3$ denotes an off-diagonal element describing the coupling between the $n+{}^7\text{Li}$ configuration with $l=3$ and the $n+{}^7\text{Li}^*$ configuration with $l=1$. The parity of this state does not need to be further specified, since it is uniquely determined by the values of l and I. In the example just mentioned, the parity is easily seen to be equal to $+1$.

As is customary, the diagonal element of the S matrix will be parametrized in terms of the reflection coefficient η_{ii}^L and the phase shift δ_{ii}^L, i.e.,

$$S_{ii}^L=\eta_{ii}^L\exp(2i\delta_{ii}^L) . \tag{5}$$

For the coupling or off-diagonal element S_{fi}^L, we shall mainly be interested in its absolute value, namely, the transmission coefficient η_{fi}^L given by

$$\eta_{fi}^L=|S_{fi}^L| . \tag{6}$$

B. Cluster internal wave functions

1. ^{7}Li Wave function

The ground state of ^{7}Li has predominantly a $t+\alpha$ cluster structure, with relative orbital angular momentum I equal to 1. In our study, both the triton and the α clusters are described by s-shell wave functions in harmonic-oscillator wells having a common width parameter $\alpha=0.514$ fm^{-2}. The $t+\alpha$ relative-motion function is taken to be

$$\chi_7(\mathbf{r}_{34})=[\exp(-\tfrac{6}{7}\eta_7\alpha r_{34}^2)+c_7\exp(-\tfrac{6}{7}\zeta_7\alpha r_{34}^2)]r_{34}Y_{1M}(\hat{\mathbf{r}}_{34}) , \tag{7}$$

with

$$\eta_7=0.185,\quad \zeta_7=0.77,\quad c_7=1.930 . \tag{8}$$

The preceding parameter values are obtained by carrying out a variational calculation, subject to the constraint that the empirical charge-form-factor data be reasonably reproduced. With this ^{7}Li wave function, the $t+\alpha$ cluster separation energy is 3.24 MeV, which is rather close to the empirical value of 3.17 MeV obtained by performing a spin-orbit averaging of the experimentally determined cluster separation energies[9] in the ground and first-excited states of ^{7}Li and by making a Coulomb correction of 0.86 MeV.

It is also found that, with a strict variational procedure without the charge-form-factor constraint, the optimum cluster separation energy obtained with a flexible five-Gaussian trial function for χ_7 is 3.28 MeV, a value very close to the above-mentioned value of 3.24 MeV. This shows that the variational stability condition for ^{7}Li is reasonably satisfied. As has been emphasized previously,[1] this is an important requirement for a nucleus involved in the incident channel when the calculation utilizes a large model space to adequately describe the behavior of the nuclear system in both the strong interaction and the channel regions.

A comparison between calculated and experimental[17] results for the square of the charge form factor F_{ch} is shown in Fig. 1. Here one sees that the agreement is good. The calculated values of the rms charge radius R_{ch}

TABLE I. Model space considered.

Model space	Cluster configurations
Single configuration (SC)	$n+{}^7\text{Li}$
Double configuration 1 (DC1)	$n+{}^7\text{Li}$, $t+{}^5\text{He}$
Double configuration 2 (DC2)	$n+{}^7\text{Li}$, $n+{}^7\text{Li}^*$
Triple configuration (TC)	$n+{}^7\text{Li}$, $t+{}^5\text{He}$, $n+{}^7\text{Li}^*$
Quadruple configuration (QC)	$n+{}^7\text{Li}$, $t+{}^5\text{He}$, $n+{}^7\text{Li}^*$, ${}^4\text{H}+\alpha$

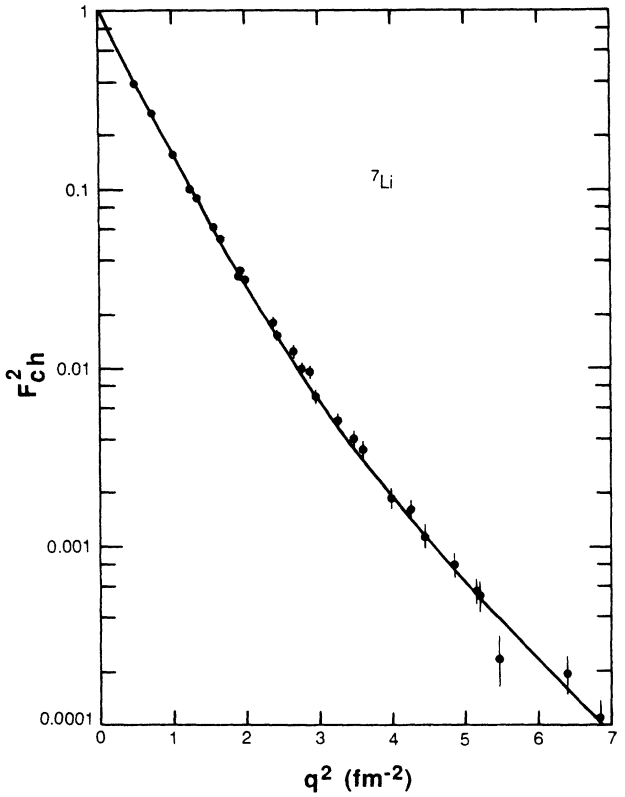

FIG. 1. Comparison of calculated and experimental results for the square of the ^{7}Li charge form factor. Experimental data shown are those of Ref. 17.

and the spectroscopic quadrupole moment Q are equal to 2.37 fm and -3.46 fm^2, respectively. These also agree quite well with the empirical value for R_{ch} of 2.37±0.05 fm obtained by averaging the values of 2.35±0.1 fm (Ref. 18) or 2.39±0.03 fm (Ref. 17) deduced from experimental measurements, and the empirical value for Q of -3.70±0.08 fm^2 (Ref. 19) obtained recently by Weller *et al.*

Using the ^{7}Li wave function $\tilde{\phi}_7$ ($I=1$), one can compute the reduced width amplitude[20] $\tilde{y}_I$ defined as

$$\tilde{y}_I(r)=\left[\begin{bmatrix}7\\3\end{bmatrix}\right]^{1/2}\left\langle\phi_t\phi_\alpha\frac{1}{r_{34}}\delta(r_{34}-r)Y_{I0}(\hat{\mathbf{r}}_{34})\tilde{\xi}_7\tilde{Z}_7\middle|\tilde{\phi}_7\right\rangle , \tag{9}$$

where $\tilde{\xi}_7$ and $\tilde{Z}_7$ denote spin-isospin and center-of-mass functions, respectively. The result is shown in Fig. 2, where we note that $\tilde{y}_I$ has an appreciable magnitude in the surface region with r larger than about 4 fm. This demonstrates that there exists a substantial degree of $t+\alpha$ clustering in the ground state of ^{7}Li, which is in full accordance with our expectation.

2. ^{7}Li* wave function

Similar to the ^{6}Li* case discussed in Ref. 1, we utilize for ^{7}Li*, which has also predominantly a $t+\alpha$ cluster structure, a bound type $t+\alpha$ relative-motion function of the form

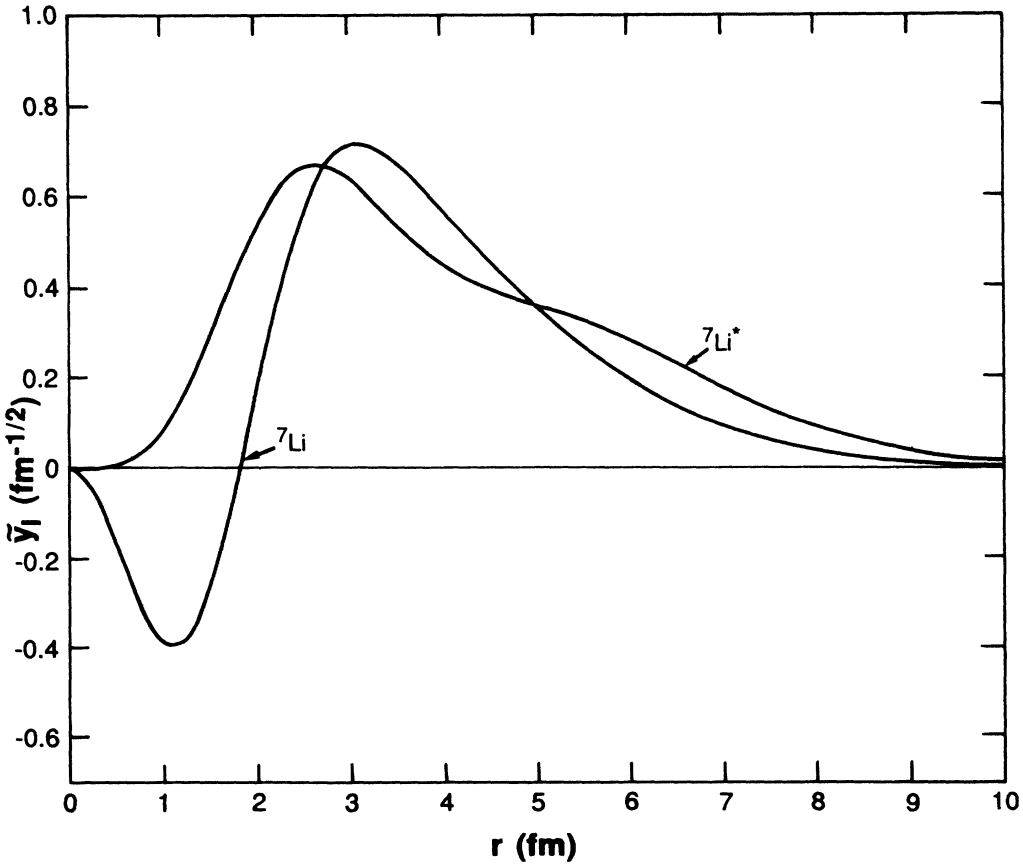

FIG. 2. Reduced width amplitudes for $t+\alpha$ clustering in ^{7}Li and ^{7}Li*.

$$\chi_7^*(\mathbf{r}_{34})=[\exp(-\tfrac{6}{7}\eta_7^*\alpha r_{34}^2)+c_7^*\exp(-\tfrac{6}{7}\zeta_7^*\alpha r_{34}^2)]r_{34}^3 Y_{3M}(\hat{\mathbf{r}}_{34}) . \quad (10)$$

Here again, as for ^{6}Li*, there is no well-defined and simple criterion for the determination of the parameter values and, thus, we adopt, in a similar fashion, the simplifying assumption that η_7^* and ζ_7^* be set equal to η_7 and ζ_7, respectively. The remaining parameter c_7^* is then determined variationally; the result is

$$c_7^*=0.988 . \quad (11)$$

With these parameter values, the excitation energy is calculated to be 5.73 MeV, which is close to the empirical value of 5.35 MeV obtained by averaging the measured excitation energies[9] of the $^2F_{7/2}$ and $^2F_{5/2}$ states according to spin-orbit weighting.

The reduced width amplitude $\tilde{y}_3$ is also shown in Fig. 2. From this figure, it can be easily concluded that our chosen wave function does describe the property of strong clustering for the ^{7}Li* nucleus.

3. ^{5}He wave function

The intercluster relative-motion function χ_5 in the nucleus ^{5}He, which has predominantly an $n+\alpha$ cluster structure, is given by Eqs. (14) and (15) of Ref. 1. It consists of a superposition of two Gaussian functions, with the parameters chosen to yield the correct value for the cluster separation energy. The reduced width amplitude is shown in Fig. 2(b) of Ref. 1. From that figure, one can readily see that the property of strong $n+\alpha$ clustering in ^{5}He is well represented.

4. ^{4}H wave function

The $n+t$ relative-motion function for the ^{4}H cluster, which has $I=1$, is simply taken as

$$\chi_4(\mathbf{r}_{13})=\exp(-\tfrac{3}{8}\eta_4\alpha r_{13}^2)r_{13}Y_{1M}(\hat{\mathbf{r}}_{13}) . \quad (12)$$

The parameter η_4 is adjusted to yield the correct resonance energy of the lowest $T=1$, $S=0$ or 1 state, obtained from experimental data[21] after correcting for spin-orbit and tensor effects.[22] The results are

$$\eta_4=0.463 \text{ for } S=0 , \quad =0.278 \text{ for } S=1 , \quad (13)$$

yielding resonance energies of 7.5 and 4.3 MeV for $S=0$ and 1 states, respectively.

5. Energy thresholds

In Fig. 3, calculated and experimental energy thresholds for $t+^5$He, $n+^7$Li*, and ^{4}H$+\alpha$ configurations, relative to the $n+^7$Li threshold, are shown in the extreme left and right columns, respectively. From this figure, one notes that the $t+^5$He and $n+^7$Li* thresholds lie close to each other. Indeed, it is just because of this particular feature that we have chosen to perform two double-configuration calculations, i.e., DC1 and DC2, in order to learn the relative importance of these two cluster configurations.

C. Simple shell-model considerations

To guide our thinking concerning the relative importance of the various cluster configurations, we first carry

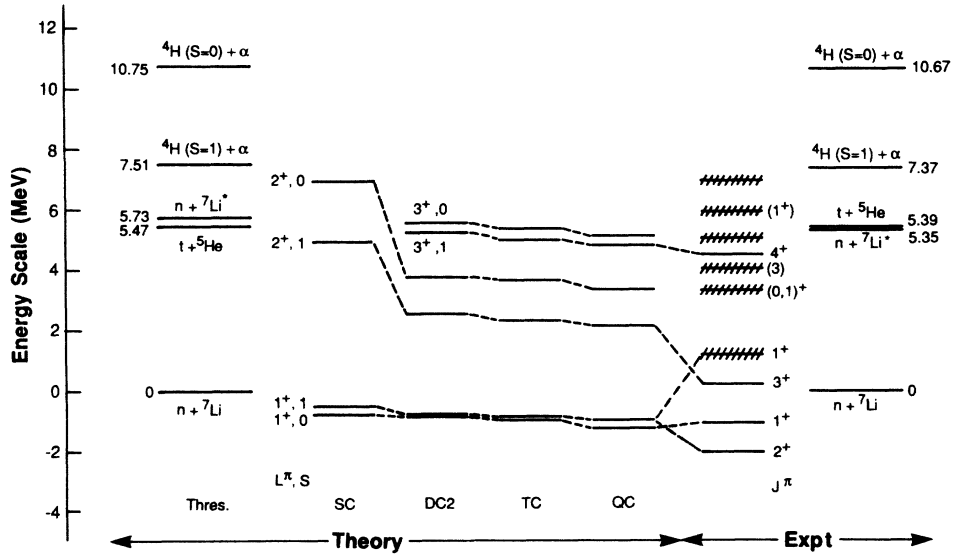

FIG. 3. Energy values of $L^\pi=1^+$, 2^+, and 3^+ states with $S=0$ or 1 obtained with SC, DC2, TC, and QC calculations, and an identification between calculated and experimental levels. Calculated and experimental threshold energies for the various cluster configurations are also shown.

TABLE II. Spectroscopic factors for $[f]=[431]$ and $(\lambda\mu)=(21)$.

Cluster configuration	l	I	Spectroscopic factor $\tilde{S}$ $L^\pi=1^+$	$L^\pi=2^+$	$L^\pi=3^+$
$n+^7$Li	1	1	1.52	0.46	0
$n+^7$Li*	1	3	0	1.06	1.52
$t+^5$He	1	1	1.21	0.36	0
$t+^5$He	3	1	0	0.85	1.21
^{4}H$+\alpha$	1	1	1.00	0.30	0
^{4}H$+\alpha$	3	1	0	0.70	1.00

out a simple consideration of ^{8}Li in the $(1s)^4(1p)^4$ oscillator shell model. For spatial symmetry $[f]=[431]$ and SU_3 symmetry $(\lambda\mu)=(21)$, states with $L^\pi=1^+$, 2^+, and 3^+ can be constructed having either $S=0$ or $S=1$. In Table II, we list the spectroscopic factors $\tilde{S}$ for these L^π states with respect to the cluster configurations adopted in this investigation. From this table, one can make the following qualitative statements.

(i) In the $L^\pi=1^+$ state, the spectroscopic factor for $n+^7$Li clustering has a large value. This indicates that, for this particular state, even a simple SC calculation is expected to yield reasonable results. Indeed, as has already been demonstrated by Descouvemont and Baye,[8] this prediction does turn out to be true.

(ii) The spectroscopic factor for the $n+^7$Li configuration is equal to zero in the $L^\pi=3^+$ state, meaning that an SC calculation would be totally inadequate. In fact, by examining the entries in this table, we can easily conclude that the $n+^7$Li* configuration must at least be included (i.e., the DC2 calculation). Again, as has been recently reported in Ref. 10, a careful investigation does fully support these predictions.

(iii) In the $L^\pi=2^+$ state, it is again not sufficient to perform a calculation which includes only the $n+^7$Li configuration. For a reliable description of this state, a multiconfiguration calculation has to be carried out.

(iv) In an overall sense, the ^{4}H$+\alpha$ configuration seems to be less important. Indeed, it is just for this reason that we have chosen to adopt a simpler, one-Gaussian relative-motion function for the ^{4}H cluster [see Eq. (12)], in order to reduce computational effort.

The fact that only $L^\pi=1^+$, 2^+, and 3^+ states can be constructed in the $(1s)^4(1p)^4$ oscillator model yields another useful prediction. It is anticipated that bound or relatively sharp resonance levels should exist only in these particular L^π states. For $L^\pi=0^+$ and 4^+, no resonances are expected and the phase-shift curves should turn out to be rather featureless in the low-energy region.

We should emphasize that the oscillator shell-model predictions given above should be considered to have mainly qualitative significance. The resonating-group trial function adopted here goes beyond the $(1s)^4(1p)^4$ oscillator model and, therefore, must be counted on to provide quantitatively reliable results. Even so, however, the information contained in terms (i)–(iv) is helpful in understanding the effects of expanding the model space on the behavior of phase shifts and level energies. This will be discussed in detail in Sec. III.

III. RESULTS FOR PHASE SHIFTS AND TRANSMISSION COEFFICIENTS

General characteristics of the phase shifts and transmission coefficients are found to be similar in $S=0$ and $S=1$ states. Hence, in the following presentation, we shall concentrate only in the $S=1$ case. For the $S=0$ case, a brief discussion will be made merely to point out some special features.

To study the roles played by the various cluster configurations, we perform the calculations in a number of different model spaces described in Table I. The results for the $n+^7$Li phase shifts and transmission coefficients as a function of E_1, the relative energy of the neutron and the nucleus ^{7}Li in the c.m. system, will be presented in graphical forms (Figs. 4–14). The calculated phase-shift values will be represented by dashed curves in the SC case, solid circles in the DC1 case, open circles in the DC2 case, crosses in the TC case, and solid curves in the QC case. For the transmission coefficients, only the results in the QC case (solid curves) will be shown. Also,

TABLE III. Bound-state and resonance energies $\tilde{E}_1(L^\pi)$ in MeV.

Model space	$L^\pi=1^+$ $S=1$	$S=0$	$L^\pi=2^+$ $S=1$	$S=0$	$L^\pi=3^+$ $S=1$	$S=0$
SC	−0.50	−0.77	4.93	6.92		
DC1	−0.66	−0.93	3.00	4.40	6.52	6.67
DC2	−0.75	−0.83	2.53	3.78	5.24	5.57
TC	−0.83	−0.95	2.31	3.67	4.99	5.38
QC	−0.96	−1.23	2.15	3.34	4.83	5.12

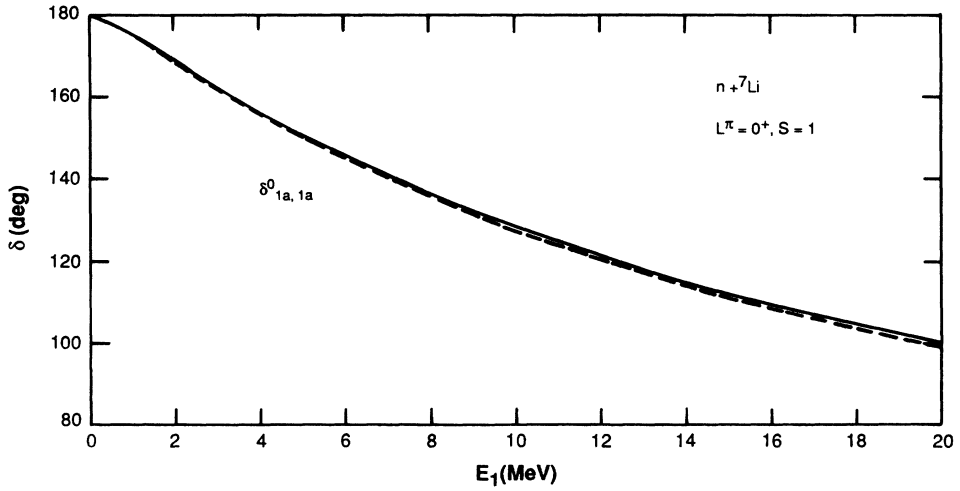

FIG. 4. Calculated phase shifts for $L^{\pi}=0^{+}$ and $S=1$ in the $n+{}^{7}\mathrm{Li}$ channel. Dashed and solid curves represent results obtained with SC and QC calculations, respectively.

for clarify in presentation, we shall not show the phase shift in any L^{π} state where its value is smaller than 5° in the considered energy range of 0–20 MeV for E_1. Similarly, when the transmission coefficient has a value smaller than 0.15 in this energy range, it will also not be presented, again for the purpose of not overcrowding the graph involved.

A. Phase-shift and transmission coefficient results in $S=1$ states

1. $L^{\pi}=0^{+}$ state (Fig. 4)

From the discussion given in Sec. II C, the $n+{}^{7}\mathrm{Li}$ phase-shift curve in this L^{π} state is expected to be rather featureless. As is seen from Fig. 4, this is indeed the case. Additionally, one also notes that the phase-shift difference between SC and QC calculations is quite insignificant, and the transmission coefficients leading from the $n+{}^{7}\mathrm{Li}$ configuration to all other configurations (not shown in Fig. 4) are small. Both of these findings indicate that the compound-nucleus region is only weakly probed by the $n+{}^{7}\mathrm{Li}$ scattering process in this state.

2. $L^{\pi}=1^{+}$ state (Fig. 5)

In this L^{π} state, the nucleus $^{8}\mathrm{Li}$ can form a bound structure. The bound-state energies, calculated in various model spaces and with the $n+{}^{7}\mathrm{Li}$ threshold set as zero on the energy scale, are given in the second column of Table III. As is seen there, the value obtained with the SC calculation is already reasonably good, which is in accordance with the oscillator-model prediction stated in item (i) of Sec. II C. The addition of other cluster configurations has some influence, but the influence is clearly rather moderate.

As is stated in Sec. II A, the exchange-mixture parameter u in the nucleon-nucleon potential is simply taken to be the same as that employed in our previous seven-nucleon study[1] (i.e., $u=1$). To see the sensitivity of our calculation with respect to this parameter, we have made several calculations, each with a different value of u. The result shows that, as u is decreased from 1.00 to 0.99, the bound-state energy of the $(L^{\pi},S)=(1^{+},1)$ state changes from -0.96 to -0.86 MeV.

Phase-shift values, shown in Fig. 5, indicate that a calculation utilizing only the $n+{}^{7}\mathrm{Li}$ configuration yields, as expected, reasonable results also at positive energies. The differences in phase shifts, obtained with SC and QC calculations, are quite small. The dispersion-like behavior

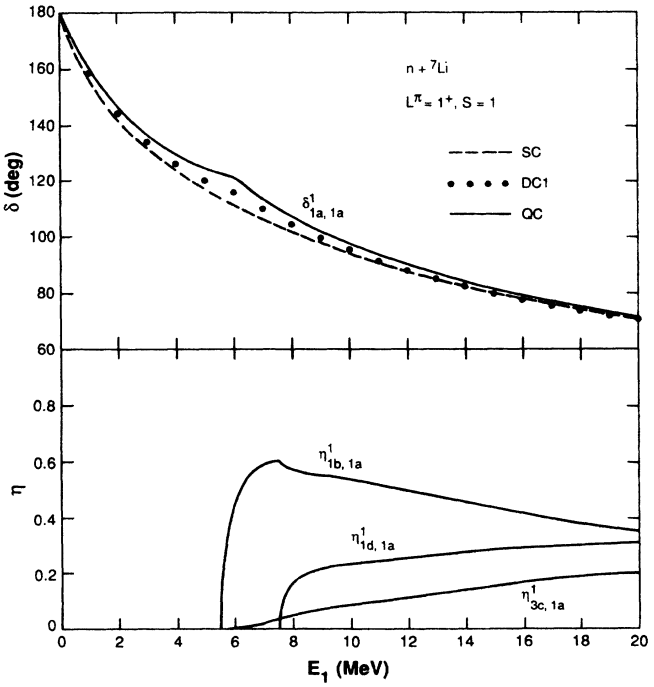

FIG. 5. Calculated phase shifts and transmission coefficients for $L^{\pi}=1^{+}$ and $S=1$ in the $n+{}^{7}\mathrm{Li}$ channel. Dashed curve, solid circles, and solid curves represent results obtained with SC, DC1, and QC calculations, respectively.

occurring at E_1 around 7 MeV arises from the presence of a resonance structure which, however, does not have predominantly an $n+^7$Li cluster configuration. From the findings that this behavior appears already in the DC1 case and there is a rather strong coupling between the $n+^7$Li and $t+^5$He configurations at about this energy (see the $\eta^1_{1b,1a}$ curve in Fig. 5), one can conclude that this structure has largely a $t+^5$He cluster configuration.

3. $L^\pi=2^+$ state (Fig. 6)

The situation in the $L^\pi=2^+$ state is very different from that in the $L^\pi=1^+$ state. From the phase-shift curves plotted in Fig. 6, one can see that the SC calculation is obviously quite inadequate [see item (iii) in Sec. II C]. The resonance energy, obtained by making a single-level analysis with a channel radius $a_c=4.3$ fm suggested in the R-matrix study of Knox *et al.*,[7] is equal to 4.93 MeV (see column 4 of Table III) in the SC case, which is much higher than the value of 2.15 MeV obtained with the QC calculation.

From Fig. 6, one additionally gains the information that, for this particular L^π state, the $n+^7$Li* configuration is more important than the $t+^5$He configuration. This is so, because the phase-shift result of the DC2 calculation is clearly better than that of the DC1 calculation, and the transmission coefficient $\eta^2_{1c,1a}$ has comparatively large values. Also, it can be seen from this figure that the $n+^7$Li, $l=3$ configuration is not very important, as indicated by the small values of $\delta^2_{3a,3a}$ in the whole energy range considered. Similarly, one can state that the inclusion of the ^{4}H$+\alpha$ configuration is not essential, because the TC and QC phase-shift results are rather similar.

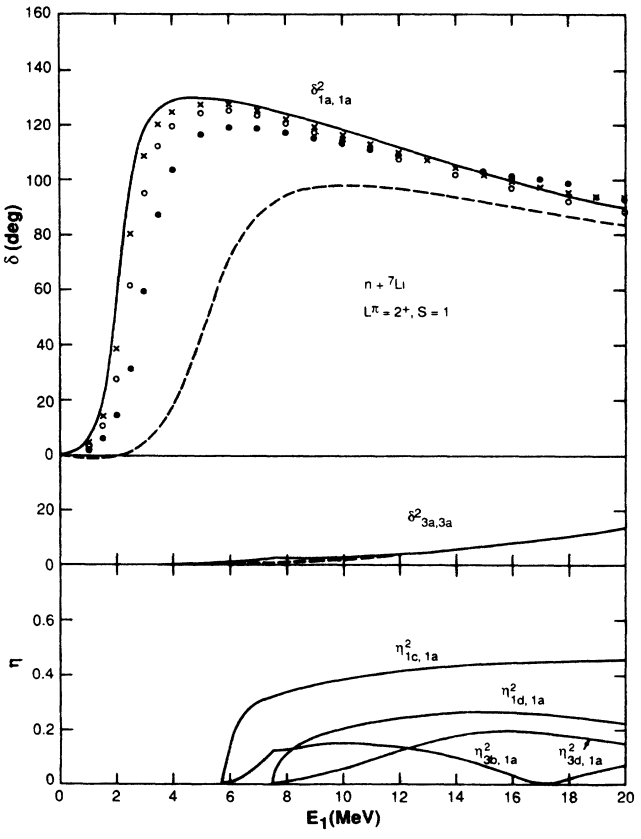

FIG. 6. Calculated phase shifts and transmission coefficients for $L^\pi=2^+$ and $S=1$ in the $n+^7$Li channel. Dashed curves, solid circles, open circles, crosses, and solid curves represent results obtained with SC, DC1, DC2, TC, and QC calculations, respectively.

4. $L^\pi=3^+$ state (Fig. 7)

Because of its particularly interesting nature, the result obtained in this state has already been published elsewhere[10] and, hence, only a brief discussion will be given here. The interesting aspect lies in the finding that the calculation yields correctly the rather unusual feature of a sharp resonance with a rather large excitation energy, in agreement with experimental observations.[9,23,24]

The SC calculation reveals no resonance structure [see item (ii) of Sec. II C], with the phase-shift values being very small in the considered energy range of 0–20 MeV. The resonance structure begins to appear with the DC1 calculation, but even here the resonance energy given in column six of Table III shows that such a multiconfiguration calculation is not yet sufficient to give an accurate description of the structure of this state. From Fig. 7 and Table III, one can readily see that this state has predominantly an $n+^7$Li* cluster structure and lies

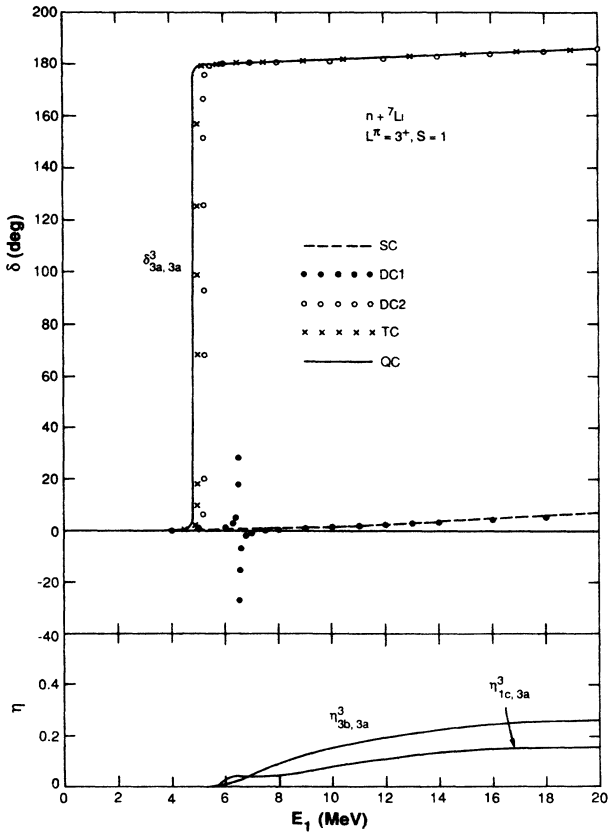

FIG. 7. Same as Fig. 6, except that $(L^\pi,S)=(3^+,1)$.

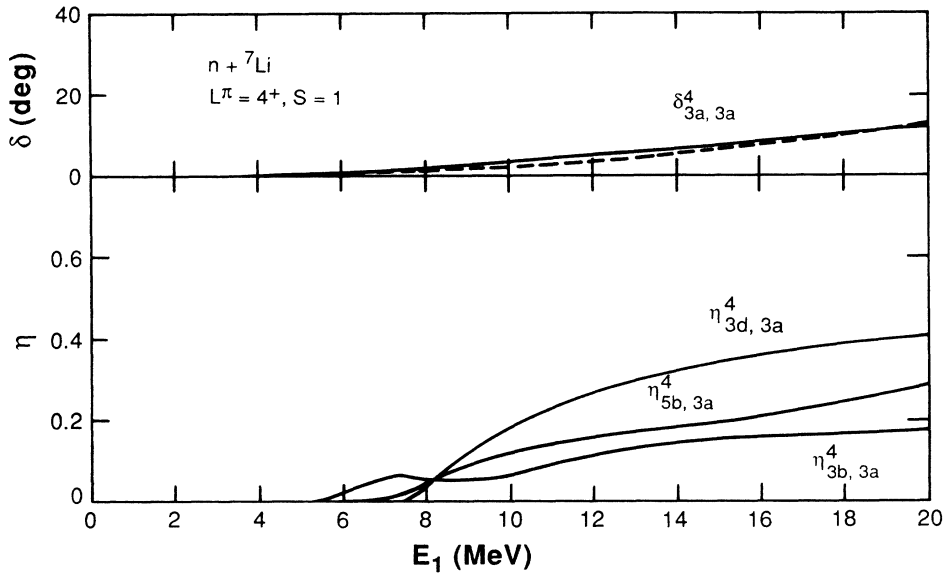

FIG. 8. Same as Fig. 6, except that $(L^{\pi},S)=(4^{+},1)$.

close to, but somewhat below, the $t+{}^5$He and $n+{}^7$Li* thresholds.

5. $L^{\pi}=4^{+}$ state (Fig. 8)

In this state, phase shift values are small and have no interesting features, as expected from the discussion given in Sec. II C. The only slightly surprising finding is that the transmission coefficient $\eta^4_{3d,3a}$, which describes the coupling between the $n+{}^7$Li and ^{4}H$+\alpha$ configurations, is larger than all other transmission coefficients. However, its value goes up to only around 0.4 even at $E_1=20$ MeV, with the consequence that the phase-shift difference between SC and QC calculations is still rather insignificant.

6. $L^{\pi}=1^{-}$ state (Fig. 9)

Both the phase shift and the transmission coefficient have complicated behavior in this state. In Fig. 9, the $n+{}^7$Li phase shifts $\delta^1_{0a,0a}$ and $\delta^1_{2a,2a}$ are shown. By analyzing these phase shifts separately[25] with single-level formulas and $a_c=4.3$ fm, we find that there exist two broad $L^{\pi}=1^{-}$ levels with resonance energies equal to 3.6 and 7.0 MeV in the QC case.

As is noted from Fig. 9, the phase-shift curves in the QC case exhibit cusp behavior at the $t+{}^5$He threshold. This is an expected phenomenon and arises from the fact that the $n+{}^7$Li configuration is coupled in a sufficiently strong way[26] to the $t+{}^5$He configuration with $l=0$ (note the rapidly rising behavior of $\eta^1_{0b,0a}$ at threshold). In addition, one also finds that the $\delta^1_{0a,0a}$ curve from the QC calculation has a dispersion-like wavy structure around 18 MeV. By studying the various transmission-coefficient curves, one can conclude that this is the result of appreciable coupling between the $n+{}^7$Li configuration in the $l=0$ state and all other cluster configurations, in particular, the $n+{}^7$Li* cluster configuration with $l=2$.

At low energies, aligned configurations with $l=L-I$ make generally the largest contribution. In this case, this is evidenced by the finding that, at energies lower than about 14 MeV, $\eta^1_{0b,0a}$ is larger than $\eta^1_{2b,0a}$ and $\eta^1_{0d,0a}$ is larger than $\eta^1_{2d,0a}$.

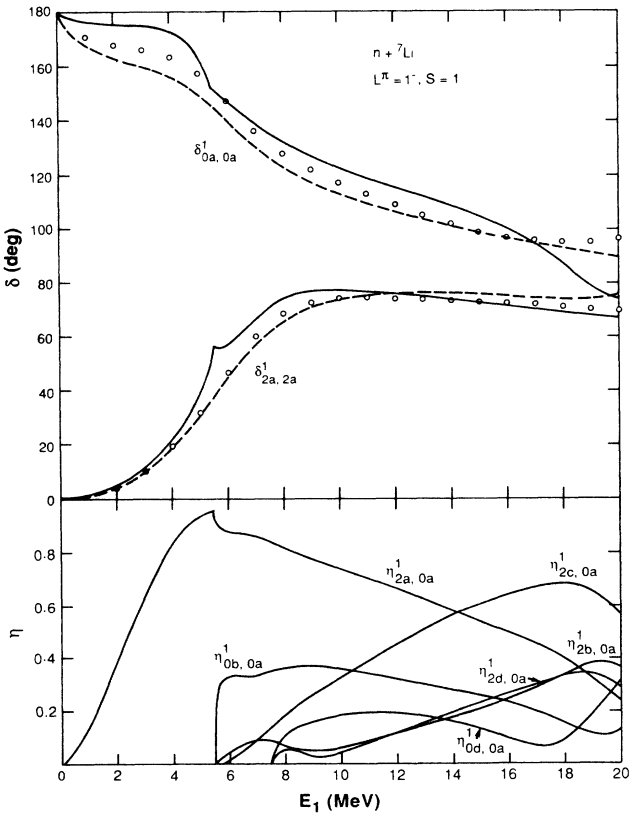

FIG. 9. Same as Fig. 6, except that $(L^{\pi},S)=(1^{-},1)$.

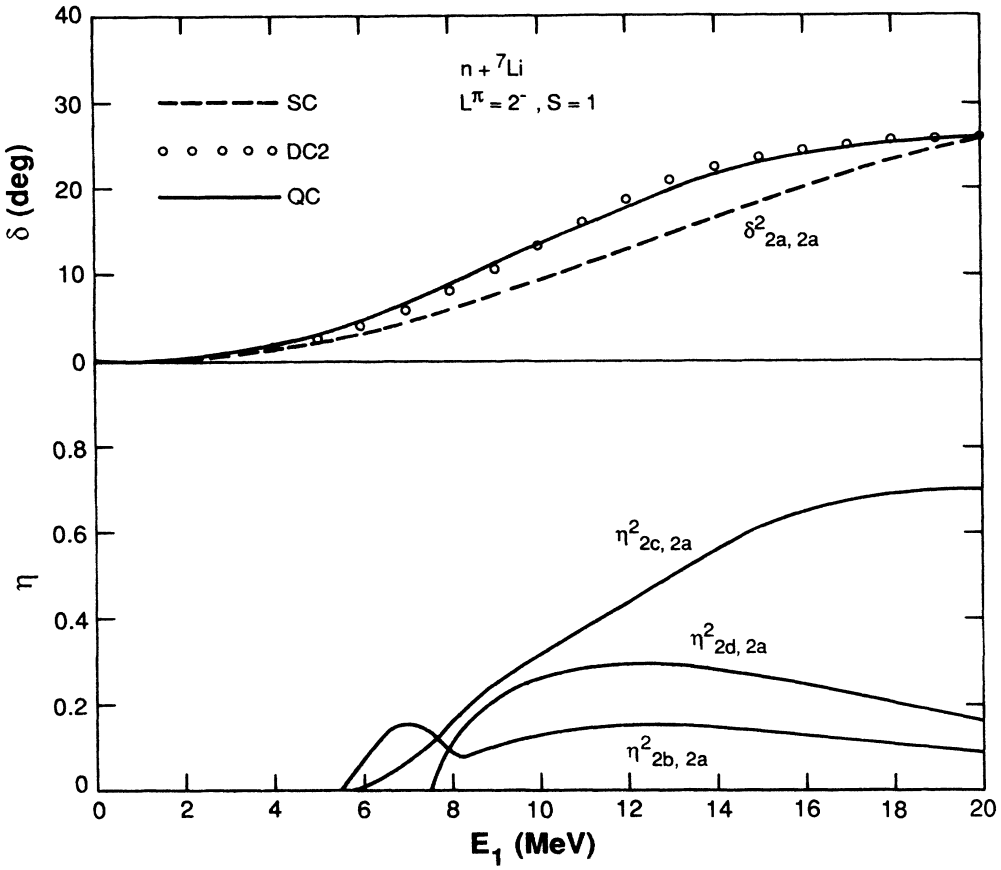

FIG. 10. Same as Fig. 6, except that $(L^{\pi},S)=(2^{-},1)$.

7. $L^{\pi}=2^{-}$ state (Fig. 10)

The features in this case are straightforward to discuss. From Fig. 10, one notes the following points:

(i) Phase-shift values are rather small throughout the whole energy region. Even at 20 MeV, the value of $\delta^2_{2a,2a}$ is only equal to about 26° in the QC case. This indicates that no significant resonance effects are expected.

(ii) The difference in phase shifts obtained from SC and QC calculations is fairly appreciable. On the other hand, the phase-shift results in the DC2 and QC cases are nearly the same. In addition, it is found that the transmission coefficient $\eta^2_{2c,2a}$ is large, especially at higher energies. All these findings suggest that the SC calculation is inadequate and the $n+{}^7\mathrm{Li}^*$ configuration must also be taken into consideration. As for the $t+{}^5\mathrm{He}$ and ${}^4\mathrm{H}+\alpha$ configurations, they seem to play minor roles in this state, as evidenced by the relatively small values for the transmission coefficients $\eta^2_{2b,2a}$ and $\eta^2_{2d,2a}$.

8. $L^{\pi}=3^{-}$ state (Fig. 11)

In the QC case, the phase shift shows a broad resonance behavior. Using a single-level analysis with $a_c=4.3$ fm, we determine the resonance energy to be

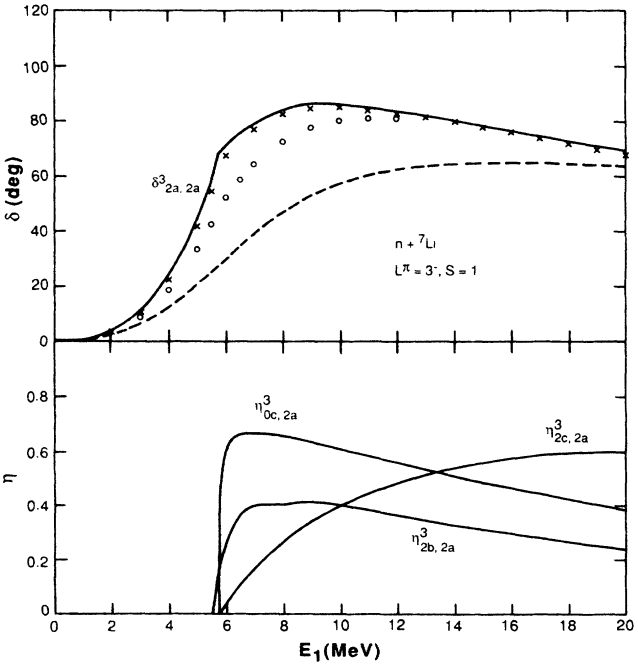

FIG. 11. Same as Fig. 6, except that $(L^{\pi},S)=(3^{-},1)$.

equal to 6.0 MeV. As for the model-space dependence of this resonance energy, we find that it is equal to 9.2, 7.2, 7.1, and 6.2 MeV in the SC, DC1, DC2, and TC cases, respectively. Thus, here again, there is a strong indication that the SC calculation is not adequate.

The QC and TC phase-shift results are very similar, indicating that the $^4H+\alpha$ configuration makes little contribution. On the other hand, these results are both significantly improved over the DC1 (not shown), DC2, and SC values. This suggests that both the $t+^5He$ and the $n+^7Li^*$ configurations are important, which is also supported by the fact that the transmission coefficients $\eta^3_{2b,2a}$, $\eta^3_{0c,2a}$, and $\eta^3_{2c,2a}$, all have rather large values.

Two other features will also be pointed out here. First, the phase-shift cusp, which shows up clearly in the TC and QC cases (much less so in the DC2 case), arises as a consequence of the coupling to the $n+^7Li^*$ configuration with $l=0$. Second, the aligned $n+^7Li^*$ configuration makes the dominant contribution in the low-energy region; at E_1 less than about 12 MeV, $\eta^3_{0c,2a}$ is seen to be significantly larger than $\eta^3_{2c,2a}$.

B. Phase-shift and transmission-coefficient results in $S=0$ states

Phase shifts for $E_1=0$ to 15 MeV in the $S=0$ state, obtained from the QC calculation, are shown in Figs. 12 and 13 for natural-parity and unnatural-parity states, respectively. Here it is seen that the general characteristics are quite similar to those in the $S=1$ state. As has already been mentioned, it is just for this reason that we choose to discuss the $S=0$ case only briefly.

Reflection coefficients for both natural-parity and unnatural-parity states are shown in Fig. 14. Here again, we should mention that the general features closely resemble those found in the $S=1$ case. We decide to plot the reflection coefficient, rather than a multitude of transmission coefficients, not for any special purpose but only to simplify the figures.

However, there is one point that is worth pointing out. From Table III we note that, out of the three positive-parity states, only the $L^\pi=1^+$ state has an energy which is lower in the $S=0$ case than in the $S=1$ case. Indeed, this special nature of the 1^+ state becomes even more transparent if we include the negative-parity states in the discussion. Single-level analyses with $a_c=4.3$ fm show, in fact, that the broad $S=0$, 1^-, and 3^- resonance levels[27] lie also above the corresponding $S=1$ levels.

The calculated binding energy of 1.23 MeV for the $S=0$, $L^\pi=1^+$ level compares quite well with the binding energy of 1.05 MeV for the $J^\pi=1^+$ level observed experimentally.[9] This is gratifying, since the exchange-mixture parameter u in the nucleon-nucleon potential is not adjusted in this calculation, but is simply set equal to the value of 1 that was found to yield satisfactory results[1] in the neighboring nuclear system ^7Li.

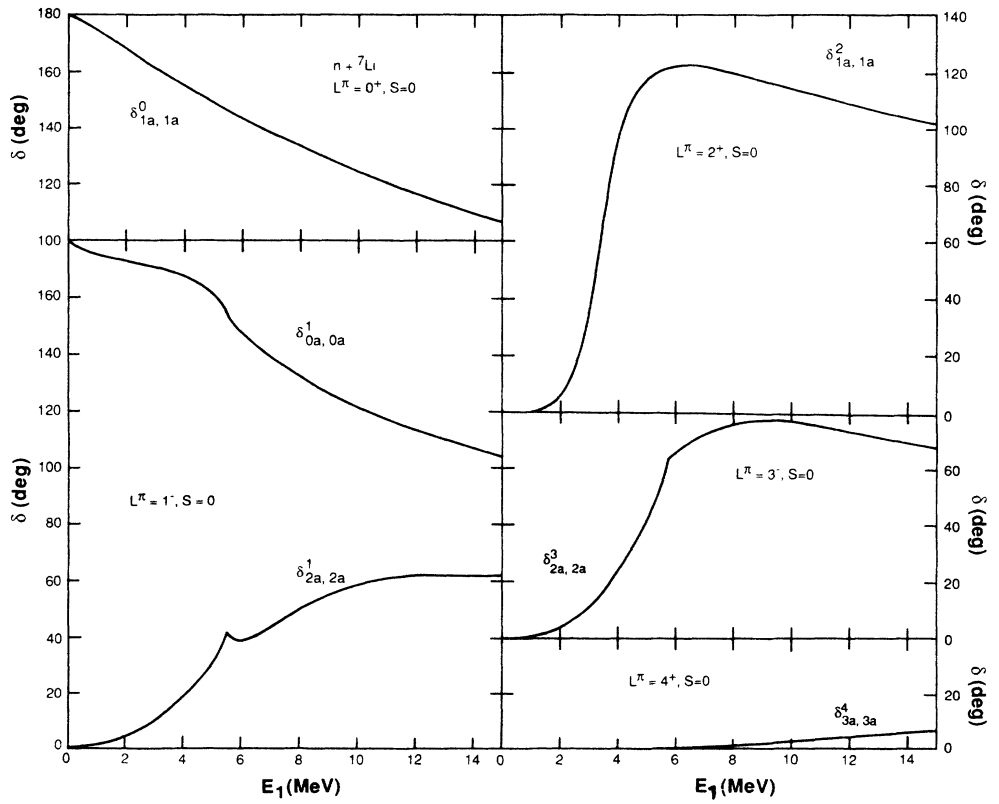

FIG. 12. Calculated phase shifts for $S=0$ natural-parity states, i.e., states with $\pi=(-1)^L$, in the $n+^7Li$ channel. Only results obtained with the QC calculation are shown.

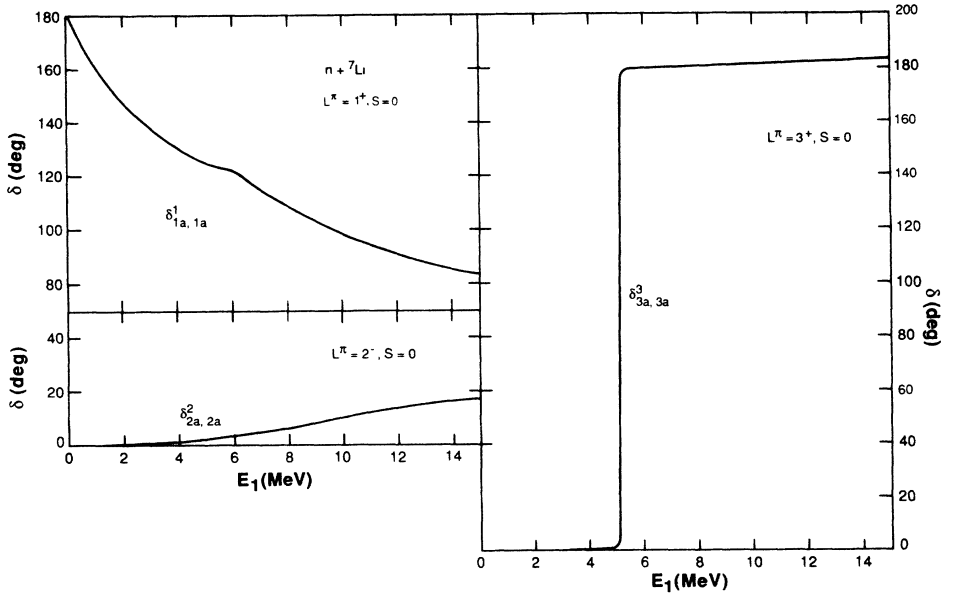

FIG. 13. Calculated phase shifts for $S=0$ unnatural-parity states, i.e., states with $\pi=(-1)^{L-1}$, in the $n+^7$Li channel. Only results obtained with the QC calculation are shown.

C. Brief summary of model-space dependence

In Fig. 3, we show the improvement in the resonance energies of the positive-parity states, as we proceed from the SC space, to the DC2 space, then to the TC space, and finally to the QC space. From this figure, one can easily see that the SC calculation is reasonably satisfactory for the $L^\pi=1^+$ states, but is quite inadequate for the description of the behavior of the $L^\pi=2^+$ and 3^+ states.

This calculation involves, in addition to the $n+^7$Li cluster configuration, the $t+^5$He, $n+^7$Li*, and ^{4}H$+\alpha$ cluster configurations. Among the latter group of configurations, the $n+^7$Li* configuration turns out to be the most important in an overall sense. Indeed, this is one of the useful lessons which we learn from this investigation. It suggests that, if an $A+B$ configuration is included in a calculation, then the configurations A^*+B, $A+B^*$, and A^*+B^*, with A^* and B^* representing rotational excited states of A and B, must in general also be taken into consideration. That this is so is supported not

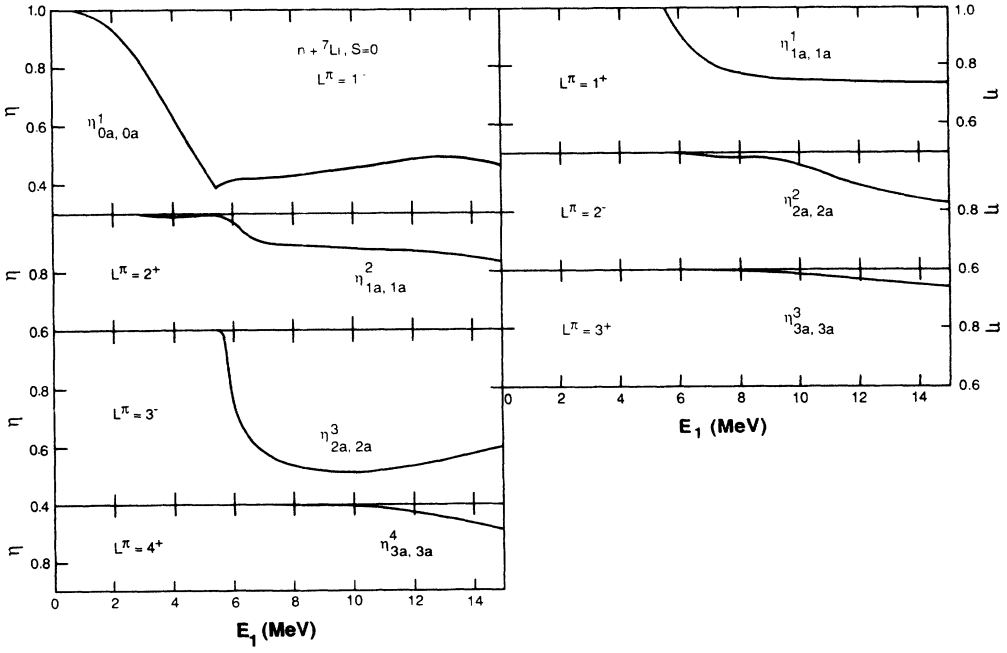

FIG. 14. Calculated reflection coefficients for $S=0$ natural-parity and unnatural-parity states in the $n+^7$ Li channel, obtained in the QC case.

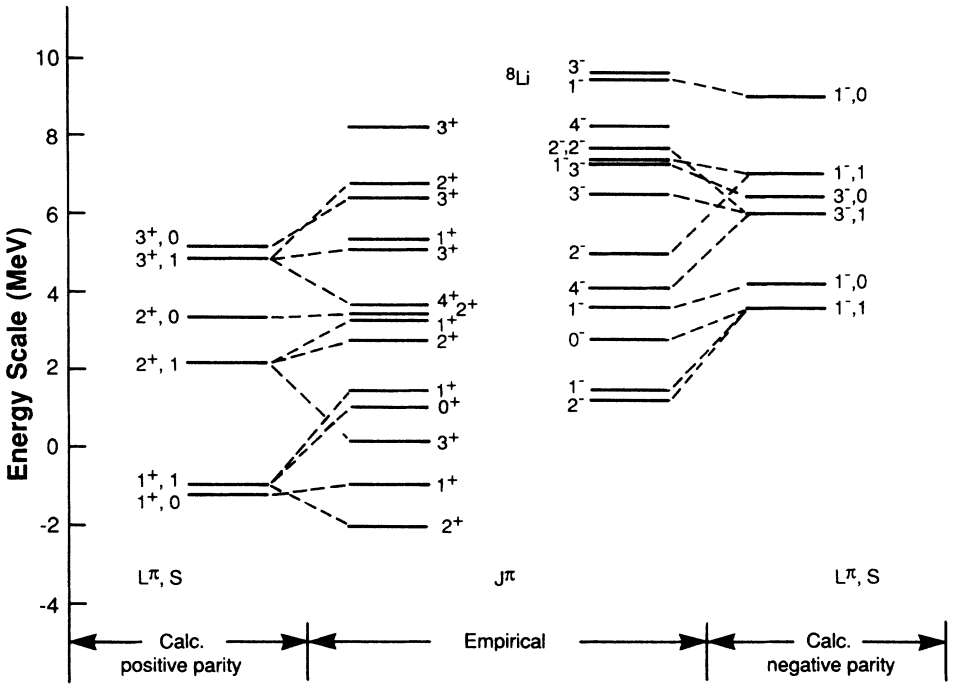

FIG. 15. A possible identification between our calculated levels and the levels obtained by Knox, Resler, and Lane (Ref. 7) based on an extensive R-matrix analysis.

only by our study of ^{8}Li, but also by our previous study[1] of ^{7}Li. In the ^{7}Li case, we have in fact found that, besides the energetically most favored $t+\alpha$ configuration, both the $n+^6$Li and the $n+^6$Li* configurations must be included in order to properly describe the behavior of this nuclear system.

The preceding finding has also practical values. For example, in a description of the nucleus ^{10}B, one might, as a first step, adopt a DC2-type calculation involving only $\alpha+^6$Li and $\alpha+^6$Li* configurations. This is a very practical simplification, since to perform an extensive ten-nucleon resonating-group calculation, similar to the one carried out here, will require a great deal of computational time and additionally also face severe numerical-accuracy problems.

D. Comparison with empirical level spectra

In ^{8}Li, only five levels have been positively identified.[9] There are the ground state with $J^\pi=2^+$, and four excited states having excitation energies of 0.98, 2.26, 3.21, and 6.53 MeV with $J^\pi=1^+$, 3^+, 1^+, and 4^+, respectively. In Fig. 3, an identification between calculated and experimental levels is attempted. To do this, we have taken consideration of the fact that noncentral effects are not included in the calculation. As is seen from this figure, there is indeed a satisfactory agreement, suggesting that when channel-coupling effects are properly considered and when realistic cluster internal functions are adopted, a good description of even the complicated eight-nucleon system can be achieved.

Next, we consider the empirical level spectrum of Knox, Resler, and Lane.[7] These authors have recently made a very careful analysis of the cross-section data using a multilevel, multichannel R-matrix study supplemented by shell-model information. In Fig. 15, we make a possible identification between our calculated and their empirical level spectra. Here one sees that there is a good correspondence for all low-lying levels, indicating that our calculation must contain all the essential ingredients.

IV. RESULTS FOR CROSS SECTIONS

A. Models-space dependence

Using calculated S-matrix elements, we can easily compute the various scattering and reaction cross sections. In Fig. 16, we show the change in $n+^7$Li differential scattering cross sections at $E_l=12.2$ MeV as the model space is changed from SC to QC. From this figure, one notes the following features:

(i) The oscillatory behavior of the SC curve is somewhat different from that of the QC curve. The second minimum is lower than the first minimum in the SC case, while the reverse is true in the QC case. Regarding this aspect, it is noted that already the DC2 cross section has the correct behavior of the QC calculation.

(ii) Differential cross sections obtained from TC and QC calculations are similar at all angles. This indicates that the ^{4}H$+\alpha$ configuration does not make an appreciable contribution to the $n+^7$Li scattering process.

(iii) Total elastic cross section obtained from the SC

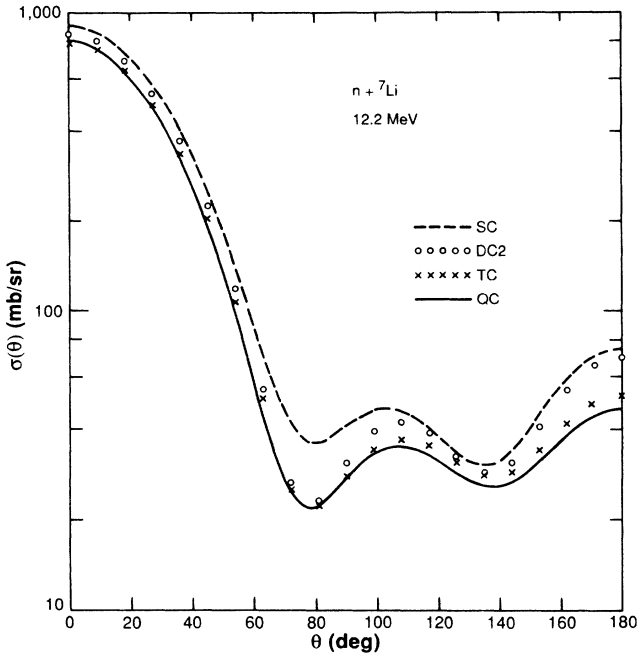

FIG. 16. Differential cross sections for $n+{}^7$Li scattering at $E_1=12.2$ MeV, obtained with SC, DC2, TC, and QC calculations.

calculation is 27% larger than that obtained from the QC calculation, suggesting again that the SC model space needs enlargement.

The DC1 result for the differential scattering cross section (not shown in Fig. 16) is distinctly better than the SC result, but is somewhat inferior to the DC2 result. This means that, from an overall viewpoint, the $n+{}^7$Li* configuration plays a more significant role than the $t+{}^5$He configuration.

B. Comparison with experiment

1. *Total reaction cross section*

In Fig. 17, we plot the $n+{}^7$Li total reaction cross section σ_R (solid curve) as a function of E_1. Additionally, contributions to individual cluster configurations $t+{}^5$He, $n+{}^7$Li*, and ^{4}H$+\alpha$ (dot-dashed curves, labeled as $a\rightarrow b$, $a\rightarrow c$, and $a\rightarrow d$) are also shown. Here one finds that the ^{7}Li$(n,n'){}^7$Li* reaction makes the largest contribution. The ^{7}Li$(n,t){}^5$He reaction has large cross sections at low energies, but becomes less important as the energy becomes higher. As expected, the ^{7}Li$(n,{}^4$H$)\alpha$ reaction turns out to be the smallest component; even so, however, its contribution to the total reaction cross section is still significant, especially at higher energies.

All the reactions considered here lead, in a sequential way, to the emission of tritons. Thus, our calculated σ_R can be compared with experimental values of the triton production cross section $\sigma_R(t)$. For example, at $E_1=12.2$ MeV, the calculated result is 286 mb. This is to be compared with the value of $\sigma_R(t)$ between about 280 and 320 mb which we obtain from the compilation of cross-section data shown in Fig. 1 of Ref. 6. Although our calculated value is at the low end of the experimental range, it is reasonable to state that there is no clear disagreement. The implication of this statement is not

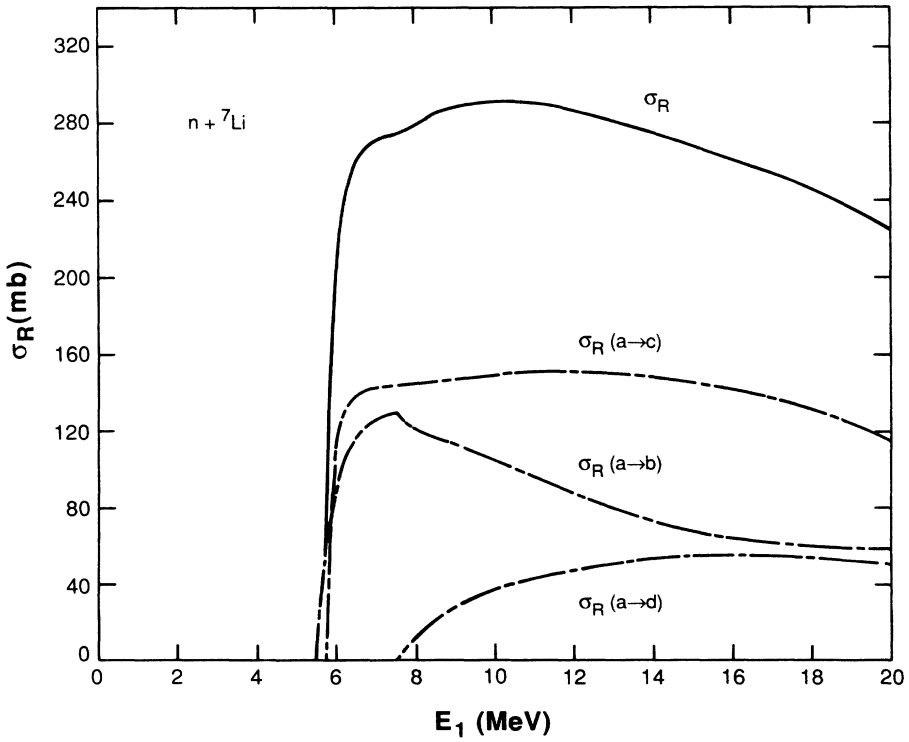

FIG. 17. Calculated $n+{}^7$Li total reaction cross section in the QC case (solid curve). Contributions from individual cluster configurations (dot-dashed curves) are also shown.

only that our study seems to be extensive enough to adequately explain the process of triton production in the $n+{}^7\mathrm{Li}$ reaction, but also that the production mechanism is mainly sequential two-body reactions. Direct three-body breakup reactions ${}^7\mathrm{Li}(n,n't)\alpha$ will contribute of course, but does not seem to have a sizable cross section—a statement which has also been advocated by Knox, Resler, and Lane.[7]

The measured value of the $n+{}^7\mathrm{Li}$ total cross section at $E_1=12.2$ MeV is 1450 mb.[28] Subtracting from this the measured value of 1064 mb for the integrated elastic cross section,[29] we obtain the experimental value of σ_R to be 386 mb. Comparing this latter value with our calculated value of 286 mb, we find that our calculation yields about 74% of the experimental total reaction cross section. Thus, even with our present rather large model space, the reaction cross section is still underestimated, although not to a large extent. The reason for this is, however, rather clear. We have omitted in our calculation a number of two-body reactions such as ${}^7\mathrm{Li}(n,d){}^6\mathrm{He}$, ${}^7\mathrm{Li}(n,2n){}^6\mathrm{Li}$, ${}^7\mathrm{Li}(n,n'){}^7\mathrm{Li}^*(7.46)$, and so on.[30] Also, direct three-body breakup reactions going into $\alpha+t+n$ and $\alpha+d+2n$ have not been considered. To remedy these shortcomings, we note that two-body reactions can be better accounted for by adding an $\alpha+d+2n$ three-cluster term into our formulation, while direct three-body reactions can be approximately included by introducing pseudoinelastic configurations[31] as has recently been done in the six-nucleon case by Kanada *et al.* These remedies will undoubtedly further improve the cross-section values, but, unfortunately, will also result in a vast increase in computational effort. For this latter reason, it is our opinion that such an ambitious endeavor should perhaps not be attempted at this moment, but should wait until more powerful computational facilities become readily available.

2. *Elastic scattering cross sections*

Differential elastic cross sections for $n+{}^7\mathrm{Li}$ scattering at 9.58 and 12.2 MeV, calculated in the QC case, are shown by solid curves in Fig. 18, where a comparison with experiment[29] is also made. Here one finds that the calculation nicely reproduces the cross sections in the forward angular region. For angles larger than 80°, the oscillatory features of the experimental results are reasonably explained, but the magnitudes of the calculated cross sections are too large, especially at backward angles beyond about 140°. We believe that this latter defect is associated with the fact that our calculated reaction cross sections are too small. With a further enlargement in model space as already suggested, we are fairly confident that the defect observed here can be largely corrected.

In Fig. 19, we show the $n+{}^7\mathrm{Li}$ integrated or total elastic cross section σ_e as a function of E_1. From this figure, we note the interesting features occurring at the thresholds of the $t+{}^5\mathrm{He}$ and $n+{}^7\mathrm{Li}^*$ channels and the influence of the $L^\pi=2^+$ and 3^+ energy levels. At energies higher than about 6 MeV, the cross-section curve is smooth and monotonically decreasing. The magnitudes

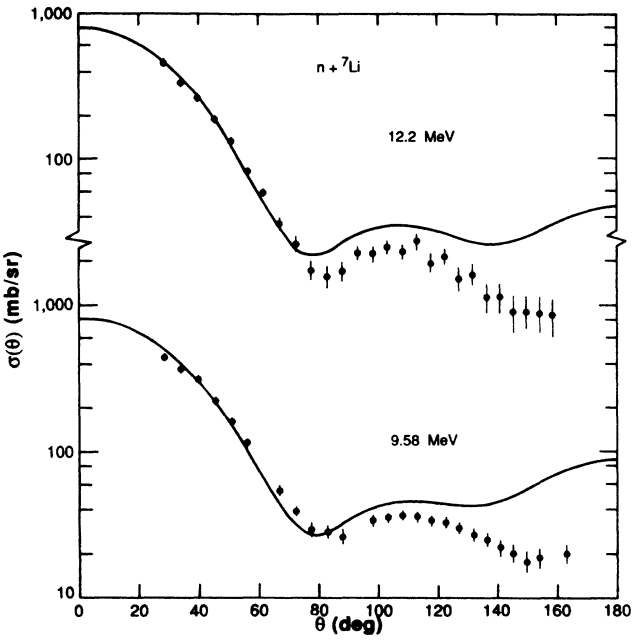

FIG. 18. Comparison of calculated $n+{}^7\mathrm{Li}$ differential scattering cross sections at 9.58 and 12.2 MeV with experiment. Data shown are those of Ref. 29.

of σ_e are 23 and 16% larger than experiment[29] (solid circles) at 6.1 and 12.2 MeV, respectively, which is again a defect associated with our finding concerning the calculated reaction cross section and points to the need of a more extensive calculation employing a larger model space.

V. CONCLUSION

In this investigation, the properties of the nucleus ${}^8\mathrm{Li}$ are examined with a multiconfiguration, multichannel resonating-group study. The model space employed is spanned by $n+{}^7\mathrm{Li}$, $t+{}^5\mathrm{He}$, $n+{}^7\mathrm{Li}^*$, and ${}^4\mathrm{H}+\alpha$ cluster configurations. To insure the reliability of the results, we have appropriately chosen the various cluster internal functions regarding their spatial characteristics. Because our major emphasis is on the energetically most-favored $n+{}^7\mathrm{Li}$ channel, the subsystem ${}^7\mathrm{Li}$ has, in particular, been carefully considered with respect to the variational stability condition, the clustering property, and the form-factor behavior.

The calculated level spectrum agrees quite well with experiment and with the empirical level spectrum obtained by Knox, Resler, and Lane[7] based on an extensive R-matrix analysis. In particular, our calculation correctly predicts the presence of a sharp ${}^3\mathrm{F}$ positive-parity resonance level with a rather large excitation energy. Considering the fact that there are *no* adjustable parameters, we may justifiably conclude that this calculation does have a basically sound foundation.

It is found that an $n+{}^7\mathrm{Li}$ single-configuration study is, in general, inadequate. Among the configurations

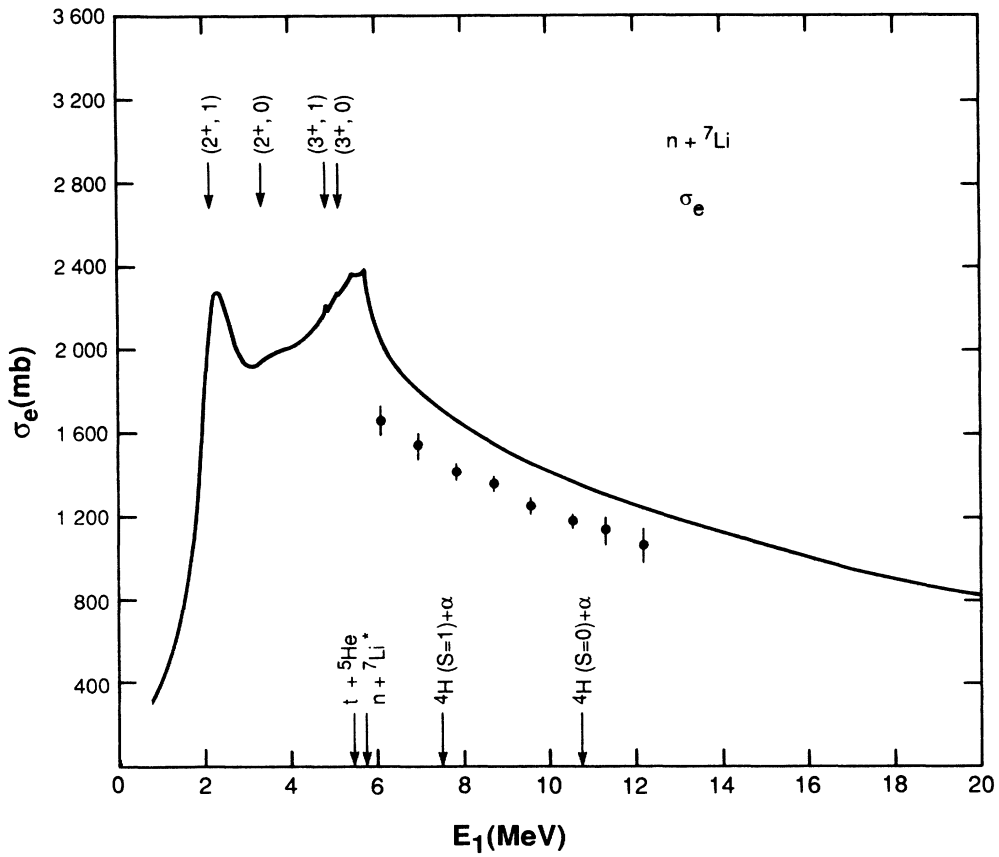

FIG. 19. Calculated $n+{}^7$Li total elastic-scattering cross section as a function of E_1. Data shown are those of Ref. 29.

$t+{}^5$He, $n+{}^7$Li*, and ^{4}H$+\alpha$ which are adopted to expand the model space, the $n+{}^7$Li* configuration is shown to be the most important in an overall sense. This is indeed one of the significant lessons that we gain from this investigation. It shows that rotational excited states of the subsystems must generally be taken into consideration.

Comparisons between calculated and experimental values on scattering and reaction cross sections have also been made. Here we find that the calculation explains all the essential characteristics of measured results. Especially the triton production cross section is well reproduced. The comparatively minor defects observed are associated with the fact that our calculated total reaction cross section is somewhat too small. Even so, however, we should emphasize that we are still getting around 75% of the experimental value, the highest percentage that has so far been obtained with microscopic resonating-group calculations containing no phenomenological imaginary potentials.

To further improve the calculated total reaction cross section will require an expansion of the model space. This can be achieved by introducing pseudoinelastic configurations and by the inclusion of an additional $\alpha+d+2n$ three-cluster term in the formulation. The introduction of pseudoinelastic configurations will pose no major problem, since a great deal of experience has already been learned in previous calculations of other light nuclear systems.[31–33] The addition of the $\alpha+d+2n$ three-cluster configuration will, however, cause both analytical and numerical difficulties. Our crude estimate is that even the computational time required will be many times larger than that needed for our calculation. Thus, even though such an improved project is undoubtedly desirable for a further, more-detailed understanding of the intricate structure of the ^{8}Li system, one must proceed slowly by first preparing the proper groundwork through the development of innovative mathematical and computational techniques.

ACKNOWLEDGMENTS

One of us (Y.F.) wishes to thank Professor S. Gasiorowicz and Professor L. McLerran for the kind hospitality extended to him at the Theoretical Physics Institute of the University of Minnesota. Also, we would like to thank the Research Center for Nuclear Physics at the Osaka University for the generous grant of computer time and the U.S. Department of Energy (Contract No. DOE/DE-AC02-79-ER10364) for financial support.

*Present and permanent address: Department of Physics, Kyoto University, Kyoto 606, Japan.
[1]Y. Fujiwara and Y. C. Tang, Phys. Rev. C **31**, 342 (1985).
[2]Y. Fujiwara and Y. C. Tang, Phys. Rev. C **32**, 1428 (1985).
[3]H. D. Knox and R. O. Lane, Nucl. Phys. **A403**, 205 (1983).
[4]Y. Fujiwara, Q. K. K. Liu, and Y. C. Tang, Phys. Rev. C **38**, 1531 (1988).
[5]Y. Fujiwara and Y. C. Tang, University of Minnesota Report UM-RGM2, 1984.
[6]See, e.g., S. M. Qaim and R. Wölfe, Nucl. Sci. Eng. **96**, 52 (1987).
[7]H. D. Knox, D. A. Resler, and R. O. Lane, Nucl. Phys. **A466**, 245 (1987).
[8]P. Descouvemont and D. Baye, Nucl. Phys. **A487**, 420 (1988).
[9]F. Ajzenberg-Selove, Nucl. Phys. **A490**, 1 (1988).
[10]Y. Fujiwara and Y. C. Tang, Phys. Lett. B **222**, 311 (1989).
[11]H. Stöwe and W. Zahn, Nucl. Phys. **A289**, 317 (1977).
[12]The analytical derivation of the three-cluster kernel for a general system composed of an α cluster and two s-shell clusters is described in detail in Ref. 5.
[13]M. Kamimura, Prog. Theor. Phys. Suppl. **62**, 236 (1977).
[14]D. R. Thompson, M. LeMere, and Y. C. Tang, Nucl. Phys. **A286**, 53 (1977).
[15]Y. Fujiwara and Y. C. Tang, Phys. Rev. C **27**, 2457 (1983); **28**, 1869 (1983); **29**, 2025 (1984).
[16]Y. C. Tang, *Microscopic Description of the Nuclear Cluster Theory*, Vol. 145 of *Lecture Notes in Physics* (Springer, Berlin, 1981).
[17]L. R. Suelzle, M. R. Yearian, and H. Crannell, Phys. Rev. **162**, 992 (1967).
[18]F. A. Bumiller, F. R. Buskirk, J. N. Dyer, and W. A. Monson, Phys. Rev. C **5**, 391 (1972).
[19]A. Weller, P. Egelhof, R. Čaplar, O. Karban, D. Krämer, K. H. Möbius, Z. Moroz, K. Rusek, E. Steffens, G. Tungate, K. Blatt, I. Koenig, and D. Fick, Phys. Rev. Lett. **55**, 480 (1985).
[20]H. J. Mang, Annu. Rev. Nucl. Sci. **14**, 1 (1964); D. Kurath, Phys. Rev. C **7**, 1390 (1973); M. Ichimura, A. Arima, E. C. Halbert, and T. Teresawa, Nucl. Phys. **A204**, 225 (1973).
[21]S. Fiarman and W. E. Meyerhof, Nucl. Phys. **A206**, 1 (1973).
[22]H. Furutani, Prog. Theor. Phys. **65**, 586 (1981).
[23]L. C. Arnold, R. N. Boyd, F. Ajzenberg-Selove, R. E. Brown, E. R. Flynn, and J. W. Sunnier, Phys. Rev. C **24**, 2326 (1981).
[24]G. B. Liu and H. T. Fortune, Phys. Rev. C **38**, 1985 (1988).
[25]This is a rather crude procedure. However, since the eigenphases are found to be not too different from the diagonal phases, we believe that the resonance energies of the broad $L^\pi=1^-$ levels are reasonably estimated.
[26]Phase-shift cusps exist also at the $^4\mathrm{H}+\alpha$ threshold. However, because of weak coupling, these cusps are not readily noticeable in the phase-shift curve of Fig. 9.
[27]In the $S=0$ state, the two broad $L^\pi=1^-$ levels have resonance energies equal to 4.2 and 9.0 MeV, respectively, while the broad $L^\pi=3^-$ level has a resonance energy equal to 6.4 MeV.
[28]D. G. Foster, Jr. and D. W. Glasgow, Phys. Rev. C **3**, 576 (1971).
[29]H. H. Hogue, P. L. von Behren, D. W. Glasgow, S. G. Glendinning, P. W. Lisowski, C. E. Nelson, F. O. Purser, W. Tornow, C. R. Gould, and L. W. Seagondollar, Nucl. Sci. Eng. **69**, 22 (1979).
[30]The reactions $^7\mathrm{Li}(n,d)^6\mathrm{He}$ and $^7\mathrm{Li}(n,2n)^6\mathrm{Li}$ do not lead to the production of tritons, while the reaction $^7\mathrm{Li}(n,n')^7\mathrm{Li}^*$ (7.46) may contribute somewhat to the triton production cross section.
[31]H. Kanada, T. Kaneko, and Y. C. Tang, Phys. Rev. C **38**, 2013 (1988).
[32]H. Kanada, T. Kaneko, and Y. C. Tang, Phys. Rev. C **34**, 22 (1986).
[33]T. Kaneko, M. Shirata, H. Kanada, and Y. C. Tang, Phys. Rev. C **34**, 771 (1986).